Distribution of Proteins Implicated in Excitation-Contraction Coupling in Rat Ventricular Myocytes

David R. L. Scriven, Pauline Dan, and Edwin D. W. Moore
Department of Physiology, University of British Columbia, Vancouver, British Columbia V6T 1Z3, Canada

ABSTRACT We have examined the distribution of ryanodine receptors, L-type Ca^{2+} channels, calsequestrin, Na^+/Ca^{2+} exchangers, and voltage-gated Na^+ channels in adult rat ventricular myocytes. Enzymatically dissociated cells were fixed and dual-labeled with specific antibodies using standard immunocytochemistry protocols. Images were deconvolved to reverse the optical distortion produced by wide-field microscopes equipped with high numerical aperture objectives. Every image showed a well-ordered array of fluorescent spots, indicating that all of the proteins examined were distributed in discrete clusters throughout the cell. Mathematical analysis of the images revealed that dyads contained only ryanodine receptors, L-type Ca^{2+} channels, and calsequestrin, and excluded Na^+/Ca^{2+} exchangers and voltage-gated Na^+ channels. The Na^+/Ca^{2+} exchanger and voltage-gated Na^+ channels were distributed largely within the t-tubules, on both transverse and axial elements, but were not co-localized. The t-tubule can therefore be subdivided into at least three structural domains; one of coupling (dyads), one containing the Na^+/Ca^{2+} exchanger, and one containing voltage-gated Na^+ channels. We conclude that if either the slip mode conductance of the Na^+ channel or the reverse mode of the Na^+/Ca^{2+} exchanger are to contribute to the contractile force, the fuzzy space must extend outside of the dyad.

INTRODUCTION

The contraction of an adult ventricular myocyte is initiated by an influx of Ca^{2+} from the extracellular space that induces the release of a much larger amount of Ca^{2+} from the sarcoplasmic reticulum (SR) (Fabiato, 1985). The most widely accepted pathway for calcium entry is the voltage-dependent L-type Ca^{2+} channel, although in recent years other pathways for calcium entry leading to release of Ca^{2+} from the SR have been proposed.

Leblanc and Hume (1990) were the first to experimentally demonstrate that the release of intracellular Ca^{2+} could be achieved without any Ca^{2+} current passing through L-type Ca^{2+} channels. They hypothesized that entry of Na^+ through voltage-gated Na^+ channels could raise the local intracellular Na^+ concentration sufficiently to produce a reversal of the Na^+/Ca^{2+} exchangers, resulting in an influx of Ca^{2+}. The amount of Na^+ entering through voltage-gated Na^+ channels is too small to produce a significant change in the bulk myoplasmic Na^+ concentration, or the reversal potential of the exchanger, unless it enters a subplasmalemmal space of restricted diffusion (fuzzy space). They therefore postulated that the voltage-gated Na^+ channels, L-type Ca^{2+} channels, ryanodine receptors, and Na^+/Ca^{2+} exchangers are all located in the fuzzy space, where ion concentrations could be significantly different from their average myoplasmic values. Recently, Santana et al. (1998) proposed that calcium could enter the cell via the sodium channel using a "slip mode" conductance. They demonstrated that this current could trigger SR Ca^{2+} release, although the amount of Ca^{2+} entering through this pathway was too small to be detected in the myoplasm.

There is considerable disagreement in the literature as to the significance of both of these pathways, whether they can contribute to EC coupling and if they occur at all. There is, as yet, no direct evidence on the positions of voltage-gated Na^+ channels, L-type Ca^{2+} channels, Na^+/Ca^{2+} exchangers, and ryanodine receptors relative to each other in the same cell. We know from immunofluorescence and immunoelectronmicroscopy that L-type Ca^{2+} channels and ryanodine receptors are co-distributed along the apposed membrane surfaces of the t-tubule and the SR, respectively (Carl et al., 1995; Sun et al., 1995). There is also good evidence that the Na^+/Ca^{2+} exchangers and the Na^+ channels are located in t-tubules and on the surface membrane (Frank et al., 1992; Kieval et al., 1992; Cohen and Levitt, 1993). Their positions relative to the location of the Ca^{2+} channels and ryanodine receptors are unknown, and therefore the potential for their interaction with other proteins within the dyadic cleft, and their participation in a restricted diffusional space, can only be inferred.

We have used indirect immunofluorescence in combination with wide-field epifluorescence microscopy, image deconvolution, and digital image analysis to identify the positions of the voltage-gated Na^+ channels, L-type Ca^{2+} channels, Na^+/Ca^{2+} exchangers, and ryanodine receptors relative to each other in ventricular cardiomyocytes. We show here that all of these proteins are clustered in discrete locations in the compartments in which they are distributed, and that the vast majority of Na^+ channels and Na^+/Ca^{2+} exchangers do not appear to co-localize with other components of the dyad or with each other.

Received for publication 31 March 2000 and in final form 21 July 2000.
Address reprint requests to Dr. Edwin D. Moore, Dept. of Physiology, University of British Columbia, 2146 Health Sciences Mall, Vancouver, BC V6T 1Z3, Canada. Tel.: 604-822-3423; Fax: 604-822-6048; E-mail: edmoore@interchange.ubc.ca.

0006-3495/00/11/2682/10 $2.00

MATERIALS AND METHODS

All chemicals used were obtained from Sigma (St. Louis, MO) unless otherwise noted. Animal handling was done in accordance with the guidelines of the Canadian Council on Animal Care.

Cell isolation and preparation

Myocytes were isolated from freshly excised hearts using the method of Rodrigues and Severson (1997). Briefly, adult male Wistar rats weighing 275–300 gm were sacrificed with an overdose of sodium pentobarbital. The hearts were removed, hung on a Langendorff apparatus, and perfused for 5 min at 37°C with a nominally Ca^{2+}-free physiological saline solution, PSS (in mM: 138 NaCl, 5 KCl, 0.3 KH_2PO_4, 0.3 Na_2HPO_4, 10 HEPES, 15 D-glucose, 1 creatine, 1 carnitine, pH 7.4) that had been equilibrated with 95% O_2/5% CO_2. To dissociate the cells the perfusate was switched to PSS containing 0.5 mg/ml type II collagenase and 1 mg/ml bovine serum albumin. When the heart began to soften the ventricles were removed, cut into small chunks, gently shaken to dislodge cells, and filtered through a 200 μm nylon mesh (Nitex) into fresh PSS. Small aliquots of cells were examined to ensure that they were quiescent, rod-shaped, and excluded Trypan Blue. In preparations used for analysis, at least 80% of the cells fulfilled these criteria. The cells were fixed for 10 min in freshly made 2% paraformaldehyde. The fixation was quenched by immersing the cells in 100 mM glycine (pH 7.4) for 10 min. The glycine was removed by 3 $\times$ 10 min washes in phosphate buffered saline, PBS (in mM: 137 NaCl, 8 NaH_2PO_4, 2.7 KCl, 1.5 KH_2PO_4, pH 7.4) and the cells were then permeabilized in a solution of PBS containing 0.1% Triton X-100 for 10 min. The permeabilization solution was removed with 3 $\times$ 10 min washes in PBS.

Immunolabeling

All antibodies used in this study were the generous gifts of the individuals listed below, and all have been previously characterized. A monoclonal antibody (C3-33) directed against the RyR2 isoform from Dr. Gerhard Meissner (Lai et al., 1992); an affinity-purified polyclonal antibody (CNC1) directed against the α_{1C} subunit of the voltage-activated Ca^{2+} channel from Dr. William Catterall (Hell et al., 1993); a polyclonal antibody directed against canine cardiac calsequestrin (Jorgensen and Campbell, 1984) from Dr. Kevin Campbell; monoclonal and polyclonal antibodies directed against the canine cardiac Na^+/Ca^{2+} exchanger from Dr. Ken Philipson (Frank et al., 1992); an affinity-purified polyclonal antibody against the voltage-activated Na^+ channel in rat ventricular myocardium, rH1 (Cohen and Levitt, 1993). Secondary antibodies were either goat anti-rabbit or goat anti-mouse conjugated to one of the fluorophores, fluorescein isothiocyanate (FITC), or Texas Red. These antibodies were affinity-purified and had been highly adsorbed to minimize species cross-reactivity (Jackson ImmunoResearch, West Grove, PA).

Small aliquots of cells were labeled with primary antibodies that had been diluted in antibody buffer (in mM: 75 NaCl, 18 Na_3 citrate with 2% goat serum, 1% bovine serum albumin, 0.05% Triton X-100, 0.02% NaN_3). Incubations involving both monoclonal and polyclonal primary antibodies were done simultaneously overnight in 1.5 ml polypropylene ultracentrifuge tubes on a rotating rack at ~5 rpm. Excess primary antibody was removed by rinsing the cells 3 $\times$ 10 min in a solution consisting of (in mM): 75 NaCl, 18 Na_3 citrate with 0.05% Triton X-100). The cells were then incubated in antibody buffer containing the appropriate secondary antibodies for 2 h, rinsed for 3 $\times$ 10 min with PBS, and then mounted onto frosted slides in a solution composed of 90% glycerol, 10% 10X PBS, 2.5% triethylenediamine, and 0.02% NaN_3. Small diameter (200 nm) microspheres labeled with equal amounts of FITC and Texas Red (Molecular Probes, Eugene, OR) were added to the mounting medium to act as fiduciary markers, facilitating alignment of the three-dimensional data sets. Coverslips were fixed to the slides with clear nail polish. Two sets of control experiments were performed: in one, cells were labeled with secondary antibody without having been incubated with primary antibody. In the second, cells that had been incubated with a polyclonal primary antibody were incubated with an anti-mouse secondary antibody, and vice versa.

In the experiment where the ryanodine receptor was labeled twice, both of the primary antibodies were monoclonal. After the first exposure to the primary antibody the first secondary antibody was a goat anti-mouse Fab fragment labeled with FITC, followed by a blocking step with a large excess of unlabeled goat anti-mouse Fab. After incubation with the second exposure to the primary antibody, the second fluorescent antibody was a goat anti-mouse IgG labeled with Texas Red. The control experiment skipped labeling with the second primary antibody and proceeded directly to the second secondary antibody. This allowed us to detect whether any sites on the primary antibody were not blocked by the goat anti-mouse Fab during the blocking step.

The antibody directed against the Na^+ channel does not recognize a fixed epitope and requires a different procedure from that outlined above. The dissociated cells were filtered into an equal volume of PSS containing 10 mM EGTA, pH 7.4, gently spun down (50 $\times$ *g*), and transferred to reverse-PSS (in mM: 120 KCl, 10 NaCl, 20 HEPES, 5 $MgCl_2$, 15 D-glucose, 10 EGTA, 5 MgATP, and 15 phosphocreatine). The cells were left in the buffer for 10 min and checked for viability with Trypan Blue. They were then permeabilized with 60 μg/ml saponin (Acros Organics, Fair Lawn, NJ) for 30 min at room temperature, after which they were gently spun (50 $\times$ *g*) and washed in reverse buffer to remove the saponin. The effectiveness of the saponin permeabilization was assessed with Trypan Blue. Cells were incubated with primary antibodies diluted in reverse-PSS with 2% goat serum added for 4 h at room temperature on a rotating rack. Cells were then fixed, rinsed, and labeled with fluorescently tagged secondary antibodies as described above.

Image deconvolution and analysis

Images were acquired with a Nikon Diaphot 200 inverted microscope, equipped for epifluorescence (100W Hg illumination), using a 100/1.3 glycerol immersion objective. The images were passed through a 2$\times$ projection lens, giving pixel dimensions of 122 nm $\times$ 122 nm. The image detector was a thermoelectrically cooled CCD camera, with a SITe SI502AB chip, peak QE 80%, with a 16-bit dynamic range (Photometrics, Tucson, AZ). All filter sets were narrow bandpass and specific for the chosen fluorophore (XF22, fluorescein; XF43, Texas Red, Omega, Brattleboro, VT). The fine focus of the microscope was connected to a stepping motor (AS 3004-001, Hurst, Princeton, IN), which in turn was controlled by an AST Bravo P/75 computer. The position of the objective relative to the stage was monitored with an eddy-current position sensor (Kaman Instrumentation, Colorado Springs, CO) which fed data to the computer allowing precise control of the objective position. The computer also controlled the shutters and stored and displayed the images acquired from the CCD camera. A typical image stack consisted of 40–60 serial two-dimensional images acquired through the cell at 0.25 μm intervals. The point spread function of the microscope was measured similarly using Fluospheres, 100 nm diameter, of the appropriate color (Molecular Probes). The three-dimensional data stacks were transferred to an Indigo^2 XZ workstation (Silicon Graphics, Pasadena, CA) for processing and analysis.

Images were processed as previously described (Moore et al., 1993). Briefly, each image was dark-current and background subtracted, and flat-field corrected to correct for non-uniformity in illumination and camera sensitivity across the field of view, and then submitted to an EPR client-server processor for deconvolution (Scanalytics, Billerica, MA). The deconvolution algorithm used was that developed by Carrington et al. (1990). Images of control cells were processed identically. After deconvolution the images were aligned using the fiduciary markers, and control images were used to identify a threshold intensity that eliminated >99% of the voxels in these images. This threshold intensity was applied to images

of the fully labeled cells such that voxels that fell below the threshold were set to zero, all other voxels remaining unchanged. Since the molecules whose position we are trying to identify are subresolution point sources corresponding to a single molecule or a cluster of molecules, we further reduced out-of-focus blur by cross-correlating the thresholded images with the image of the deconvolved bead that was used to measure the point spread function of the microscope. When the *z* axis fluorescence intensity profile of a spot matched the fluorescence distribution of the deconvolved bead, only the voxel that was identified as maximal in the *z* dimension was retained. Those voxels with identical *x* and *y* coordinates and a *z* coordinate ± 1 were considered to be co-localized, and a voxel in the first image was allowed to co-localize with only one voxel in the second image. The extra two voxels allowed for co-localization in *z* reflects the limited axial resolution. As a final step, and for visualization only, voxels in the second image that were identified as co-localized were moved in *z* to the co-localized position, and the images were then interpolated in *z* to produce cubic voxels.

RESULTS

Deconvolution and image analysis

Deconvolution reduced the full-width at half-maximum intensity (FWHM) of the image of a polystyrene bead labeled with Texas Red from 0.52 μm to 0.26 μm in both the *x* and *y* dimensions, and in *z* the FWHM was reduced from 1.16 μm to 0.78 μm. Comparable FWHM values for the fluorescein beads were 0.48 μm in *xy* and 1.02 μm in *z* before deconvolution and 0.25 μm in *xy* and 0.72 μm in *z* after deconvolution. Voxel dimensions of 122 nm $\times$ 122 nm $\times$ 250 nm therefore satisfy the Nyquist criteria for sampling.

In Fig. 1 we display the raw data (*A*), and the deconvolved image (*B*), of a single ventricular cell labeled with an antibody specific for the ryanodine receptor (RyR), followed by a secondary anti-mouse antibody tagged with Texas Red. The raw data (Fig. 1 *A*) had the dark-current and background intensity subtracted, and were corrected for non-uniformities in illumination intensity before being deconvolved. The deconvolved data (Fig. 1 *B*) were thresholded, after which no other image processing was done. The ryanodine receptor is located largely in the sarcoplasmic reticular membrane adjacent to the t-tubules (Carl et al., 1995; Sun et al., 1995), so the predominant labeling along the *z* lines is consistent with previous results. The sarcomere spacing was $\sim$1.87 μm, indicating that the cell was largely relaxed. In control images (not shown) in which cells were labeled with the fluorescently tagged secondary antibody alone, the image intensity was on average 9.1 $\pm$ 1.4 (mean $\pm$ SD, $n = 25$) times dimmer than the fully labeled cells. Images from control cells displayed diffuse labeling everywhere with no clear pattern, unlike the image presented in Fig. 1 *B*, where an organized pattern is clearly visible.

A closer analysis of the image revealed further details of the nature of the labeled structures. A small portion of the image surrounding one of the *z* lines, as indicated by the box in Fig. 1 *B* (24 $\times$ 16 $\times$ 52 voxels), was magnified so that individual voxels could be seen (Fig. 1 *C*). The single plane

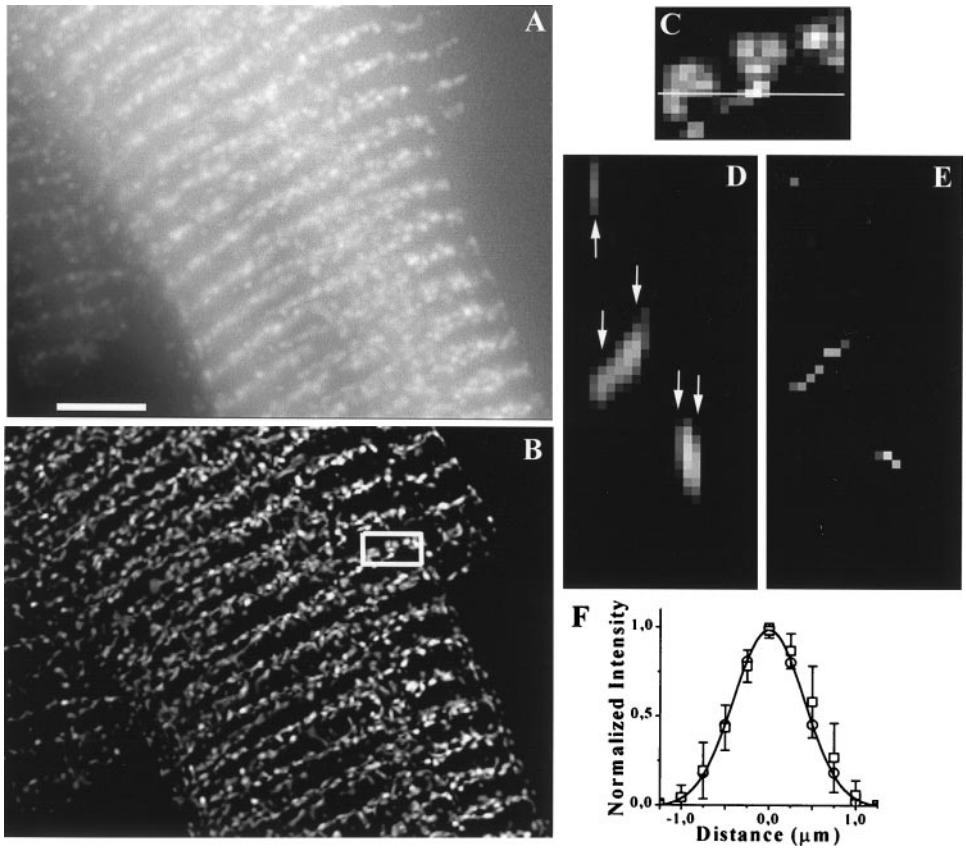

FIGURE 1 (*A*) Image obtained from wide-field microscope showing the distribution of ryanodine receptors in a ventricular myocyte. The image is a maximum intensity projection, dimensions 254 $\times$ 193 $\times$ 51 voxels. Scale bar is 5 μm. (*B*) Image *A* following deconvolution and thresholding. (*C*) Magnification of the boxed region in *B*. (*D*) The plane of voxels indicated by the white line was isolated and rotated 90° about the *x* axis. (*E*) Image *D* following cross-correlation of the deconvolved bead with the deconvolved image to isolate voxels that were maxima in the *z* axis. (*F*) Plot of the normalized intensity in the *yz* plane of a deconvolved bead (○) and the normalized fluorescence intensity of the columns of pixels indicated by the arrows in *C* (□), versus distance from the brightest pixel (mean $\pm$ SD, $n = 5$). The data were fitted with Gaussian curves.

of voxels indicated by the white line was then isolated, rotated on the *x* axis, and the resulting single *xz* plane displayed (Fig. 1 *D*). We then compared the normalized intensity along the *z* axis (the voxel with the highest intensity was set to distance zero) of the columns of fluorescence indicated by the arrows, with that of a deconvolved bead labeled with Texas Red. The results are plotted in Fig. 1 *F*, and it is evident from the graph that the profiles of the intensities of the deconvolved bead and the spots of specific fluorescence in the deconvolved image were not significantly different. The same result was obtained in all of the images that we have examined, regardless of the epitope tagged or the fluorophore used. These results indicate that spots of specific fluorescence in the deconvolved images behave as though they were subresolution points with a small amount of out-of-focus haze remaining after the deconvolution. We therefore cross-correlated the deconvolved image of the bead labeled with Texas Red with the deconvolved image of the ryanodine receptor distribution to identify those points, along the *z* axis, most likely to contain specific signal. The results of this process are displayed in Fig. 1 *E*. Unless otherwise stated, all of the images analyzed and displayed were treated in the same manner.

Co-localization

The principal aim of this study was to determine if the Na^+/Ca^{2+} exchanger and the voltage-activated Na^+ channel were positioned on the membrane of the t-tubules adjacent to dyadic couplings of ryanodine receptors and L-type Ca^{2+} channels. To achieve that goal cells were labeled with antibodies specific for the proteins whose location we were interested in examining, and the two three-dimensional data sets were then processed and merged. Since a cell could rarely be viewed in its entirety under high power, sections from the centers of cells that were well-labeled with both fluorophores were selected for analysis. When comparing two images the requirements for co-localization were strict. Only those voxels that had identical *x* and *y* coordinates and a *z* coordinate of ± 1 voxel were considered to be co-incident. This forced any errors in co-localization to be errors of omission, not errors of inclusion; only those voxels that were truly co-localized were counted as co-incident. The results are presented graphically in Fig. 2, and numerically in Table 1. The images are binary; the protein was either present in a given voxel, i.e., its intensity was above threshold, or it was not. Voxels are one of red (protein with Texas Red label), green (protein with FITC label), white (proteins were co-localized), or black if neither protein was there.

In Fig. 2 *A* we display a stereo-pair of images of a cell labeled with antibodies specific for the α_{1C} subunit of the L-type Ca^{2+} channel (green) and the ryanodine receptor (red). Both were distributed almost completely along *z* lines, with a sarcomere spacing of 1.85 μm in this image pair. There was little labeling, and few dyads, located between the *z* lines, and therefore few peripheral couplings. The abundance of white voxels implies that most of the α_{1C} subunit of the L-type Ca^{2+} channel was co-incident with ryanodine receptors, and the numerical analysis presented in Table 1 confirms the visual impression: in five pairs of similarly labeled images, 56.7% of the voxels identified as containing the α_{1C} subunit of the L-type Ca^{2+} channel also contained the ryanodine receptor, but only 36.7% of the voxels containing ryanodine receptor contained the L-type Ca^{2+} channel, and these values are significantly different from each other ($p < 0.05$). This difference in the extent of co-localization between this pair of proteins is the result of there being a much larger number of voxels that were identified as containing ryanodine receptor (17,887 voxels in five images) than voxels containing the α_{1C} subunit of the L-type Ca^{2+} channel (10,982 voxels). This is also evident from the images in Fig. 2 *A*, in which a considerable abundance of red voxels can be seen. Since there is overwhelming evidence (Carl et al., 1995; Sun et al., 1995) that the L-type Ca^{2+} channel and the RyR are located opposite each other in the membranes of the t-tubule and the SR, respectively, one might expect that the calculated co-localization values would be higher.

We therefore determined the maximum amount of co-localization that could be measured under our optical conditions and with these labeling techniques. Cells were incubated with the ryanodine receptor antibody twice (see Methods); binding an FITC-conjugated secondary after the first incubation and a Texas Red secondary after the second incubation. As the results in Table 1 show, there was no significant difference in the amount of co-localization between the first and second exposure to the primary antibody, indicating that under the conditions of this experiment the epitopes were not saturated following the first exposure to the primary antibody. This experiment defines the empirical limit of co-localization, ~63%, and reflects both a random residual mismatch between the image pairs when they are aligned to the nearest voxel and the chemical limitations of labeling proteins with antibodies. Given these limitations, the number of voxels containing the α_{1C} subunit of the L-type Ca^{2+} channel, which also contained the ryanodine receptor, is not significantly different ($p < 0.05$) from the empirical maximum that we can record with this technique.

Co-localization values similar to those measured for the L-type channel and ryanodine receptor were obtained when examining images labeled with antibodies specific for calsequestrin and the ryanodine receptor (Fig. 2 *B*, Table 1). The stereo-pair displayed in Fig. 2 *B* indicates that most of the label specific for calsequestrin was located at, or close to, the *z* lines, as was the ryanodine receptor. The two proteins also appear to be largely co-localized, and numerical analysis confirmed this impression; in five image pairs examined, 61.6% of the voxels containing calsequestrin also contained ryanodine receptors, while 55.8% of the voxels

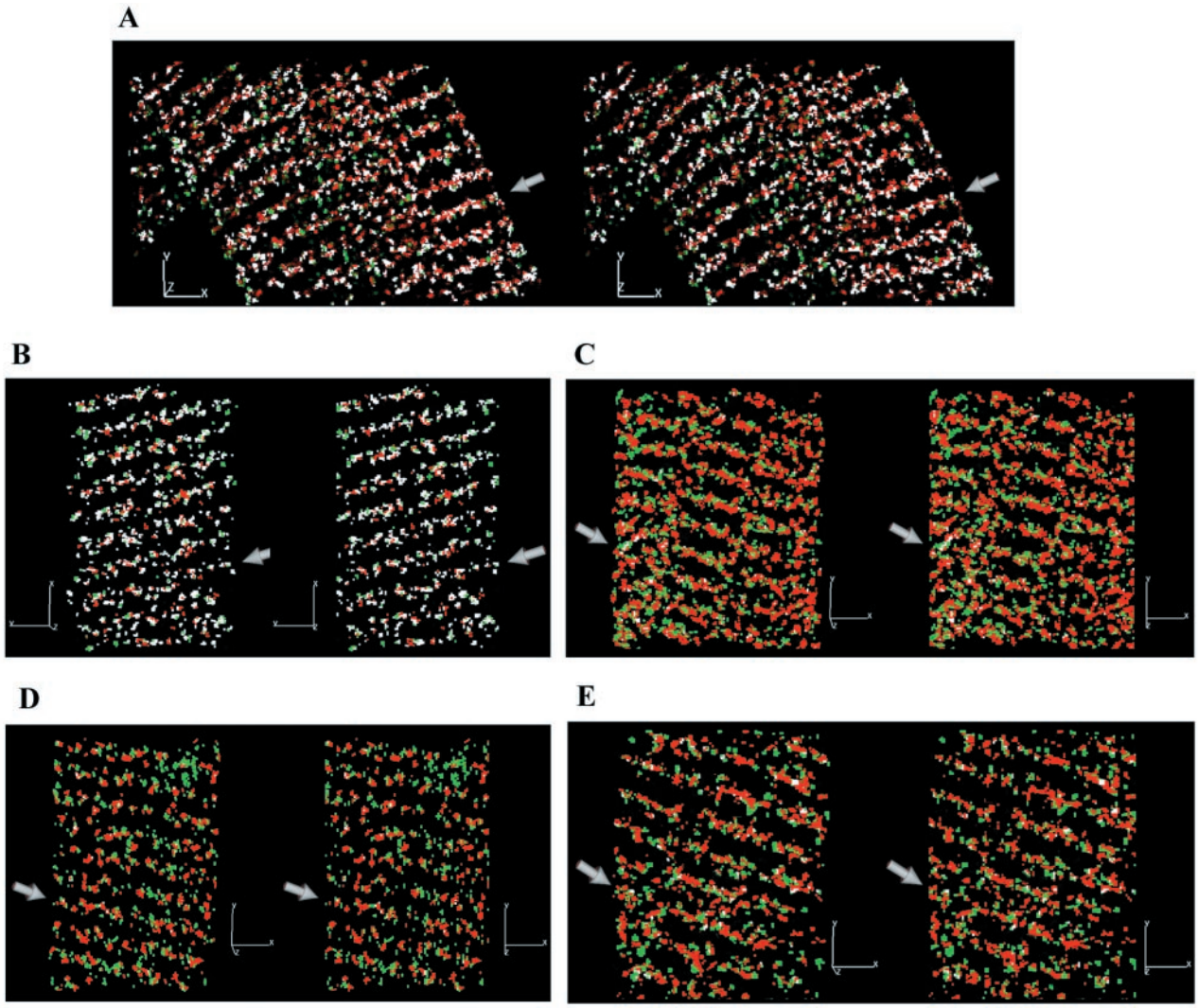

FIGURE 2 (*A*) Stereo-pair showing a myocyte segment (size, in pixels: 225 × 119 × 51) labeled with antibodies against the α_{1C} subunit of the L-type Ca^{2+} channel (*green*) and the ryanodine receptor (*red*). The large arrow points to the surface of the cell and a presumed *z* line. If the pixel is white, then both proteins occupy that pixel. Scale bar is 2.44 μm in the *x*, *y*, and *z* directions in this and subsequent images. (*B*) Stereo-pair (132 × 83 × 28) showing the distribution of calsequestrin (*green*) and the ryanodine receptor (*red*). (*C*) Stereo-pair (110 × 135 × 25) of the Na^+/Ca^{2+} exchanger (*green*) and the ryanodine receptor (*red*). (*D*) Stereo-pair (88 × 134 × 24) of the voltage-gated Na^+ channel (*green*) and the ryanodine receptor (*red*). (*E*). Stereo-pair (149 × 131 × 24) of the voltage-gated Na^+ channel (*green*) and the Na^+/Ca^{2+} exchanger (*red*).

containing ryanodine receptors also contained calsequestrin. These values were not significantly different from each other nor from the theoretical maximum amount of co-localization previously measured. The number of voxels containing the ryanodine receptor that also contained calsequestrin was significantly greater ($p < 0.05$) than the num-

TABLE 1 Co-localization of pairs of the indicated proteins

Protein A (FITC Label)	Protein B (Texas Red Label)	Co-Localization (%)		*n*
		A with B	B with A	
Ca^{2+} Channel (10,982)	Ryanodine Rec. (17,887)	56.7 ± 5.1	36.7 ± 4.8	6
Calsequestrin (19,516)	Ryanodine Rec. (21,147)	61.6 ± 7.2	55.8 ± 6.2	5
Na^+/Ca^{2+} Exchanger (40,020)	Ryanodine Rec. (30,444)	5.8 ± 1.9	7.7 ± 2.3	5
Na^+ Channel (19,645)	Ryanodine Rec. (18,591)	2.9 ± 0.9	3.1 ± 1.2	4
Na^+/Ca^{2+} Exchanger (23,619)	Na^+ Channel (23,021)	3.5 ± 1.5	3.6 ± 2.1	6
Ryanodine Rec. (14,341)	Ryanodine Rec. (15,162)	64.7 ± 5.8	61.2 ± 5.7	5

The numbers in parentheses represent the total number of voxels labeled with the protein in *n* cell segments.

ber of voxels containing the ryanodine receptor, which also contained the α_{1C} subunit of the L-type Ca^{2+} channel.

We next investigated whether the Na^+/Ca^{2+} exchangers and the voltage-activated Na^+ channels are situated in the dyads, which would be required for reverse operation of the Na^+/Ca^{2+} exchanger to be an effective mediator of Ca^{2+} influx and therefore of EC coupling. We labeled cells with antibodies specific for the Na^+/Ca^{2+} exchanger and the ryanodine receptor (Fig. 2 *C*). There is very little co-localization apparent in this image, although both proteins were distributed largely in the area presumed to be the *z* line. Of the 40,020 voxels identified as containing a signal specific for the Na^+/Ca^{2+} exchanger and 30,444 voxels specific for the ryanodine receptor in five cells, only 2331 voxels contained both proteins. This indicates that only 5.8% of the voxels containing Na^+/Ca^{2+} exchanger also contained ryanodine receptor, and only 7.7% of the voxels containing ryanodine receptor also contained Na^+/Ca^{2+} exchanger (Table 1). These co-incidence values are significantly less than the co-incidence values recorded for either the ryanodine receptor/α_{1C} subunit of the L-type Ca^{2+} channel or the ryanodine receptor/calsequestrin image pairs ($p < 0.05$). While few Na^+/Ca^{2+} exchangers in the sarcolemma were positioned adjacent to ryanodine receptors in the SR, it was still possible that the voltage-gated Na^+ channels were in the dyads and could contribute to Ca^{2+} influx via slip mode conductance.

We therefore examined the extent of co-localization between the voltage-gated Na^+ channel and the ryanodine receptor, the results of which are presented in Fig. 2 *D* and in Table 1. The visual impression, confirmed by the numerical analysis, is that there is little co-incidence between these two proteins. Of the 18,591 voxels that contained the ryanodine receptor and the 19,645 voxels that contained the voltage-gated Na^+ channel in the four cells examined, only 576 voxels were considered co-incident. This result indicates that 2.9% of the voxels containing the Na^+ channel also contained the ryanodine receptor while 3.1% of the voxels containing the ryanodine receptor also contained the Na^+ channel. These values are significantly less ($p < 0.05$) than the co-localization values recorded for ryanodine receptor/L-type Ca^{2+} channel or the ryanodine receptor/calsequestrin image pairs.

In some smooth muscle cells the Na^+/Ca^{2+} exchanger is positioned on the sarcolemma adjacent to the Na^+/K^+ pump (Moore et al., 1993). This arrangement was thought to allow rapid and reciprocal responses to changes in the intracellular Na^+ concentration by these two proteins. It was therefore of interest to determine whether the Na^+/Ca^{2+} exchanger and the voltage-gated Na^+ channel, neither of which has significant presence within the dyadic cleft, could be co-positioned elsewhere along the t-tubular membrane. This arrangement would allow the Na^+/Ca^{2+} exchanger to respond rapidly to local changes in $[Na^+]_i$.

A stereo-pair of images of the distribution of the Na^+/Ca^{2+} exchanger and the voltage-gated Na^+ channel, shown in Fig. 2 *E* with the numerical analysis in Table 1, indicates that these proteins occupy separate regions within the t-tubule membrane. Also readily apparent in this image is the presence of both proteins in areas of the cell distant from the *z* lines (indicated by the arrow) which are most likely longitudinal elements of the t-tubules. This distribution was not observed for the ryanodine receptor, calsequestrin, or the L-type Ca^{2+} channel. In the six cells examined, 23,021 voxels contained signal specific for the voltage-gated Na^+ channel and 23,619 contained signal specific for the Na^+/Ca^{2+} exchanger, but only 825 voxels contained both proteins.

Epitope labeling

Examining a thin 1 μm section of an image of a cell labeled with a single antibody revealed additional details of the pattern of distribution of the epitope that were not readily apparent from the 3D data sets (Fig. 3 *A*). The ryanodine receptor was distributed in a regular array with rows of fluorescent spots distributed along the *z* lines and in columns running parallel to the long axis of the cell. The columns were 0.98 μm $\pm$ 0.16 μm apart, which corresponds roughly to the diameter of a myofibril (Toffolo and Ianuzzo, 1994). No label was observed elsewhere in the cell, and little on the cell surface on regions outside of the *z* lines, indicating that peripheral couplings are few in number and probably have no significant role in EC coupling in adult cardiomyocytes. A similar pattern of distribution was observed for both the α_{1C} subunit of the L-type Ca^{2+} channel (Fig. 3 *B*) and calsequestrin (Fig. 3 *C*). The labeling pattern of the Na^+/Ca^{2+} exchanger and the Na^+ channel shared some of these characteristics, e.g., discrete localization and labeling along the *z* lines (Fig. 3, *D* and *E*), but both also displayed longitudinally oriented spots of fluorescence, which is also apparent in the stereo-pairs (Fig. 2, *C–E*).

DISCUSSION

In this study we have directly examined the molecular constituents of coupling regions between sarcolemma/t-tubule and SR in adult rat ventricular myocytes. We chose the rat myocyte for study since there is evidence both in favor of (Levi et al., 1993; Wasserstrom and Vites, 1996), and against (Sham et al., 1992; Bouchard et al., 1993; Satoh et al., 2000), the hypothesis that reverse mode operation of the Na^+/Ca^{2+} exchanger induces release of Ca^{2+} from internal stores. In addition, the only report of slip mode conductance of voltage-gated Na^+ channels is in rat myocardium (Santana et al., 1998). Our principal conclusion is that only the L-type Ca^{2+} channel and the ryanodine receptor are in close proximity to each other in the apposed membranes. Furthermore, the differential distribution of Na^+/Ca^{2+} exchangers

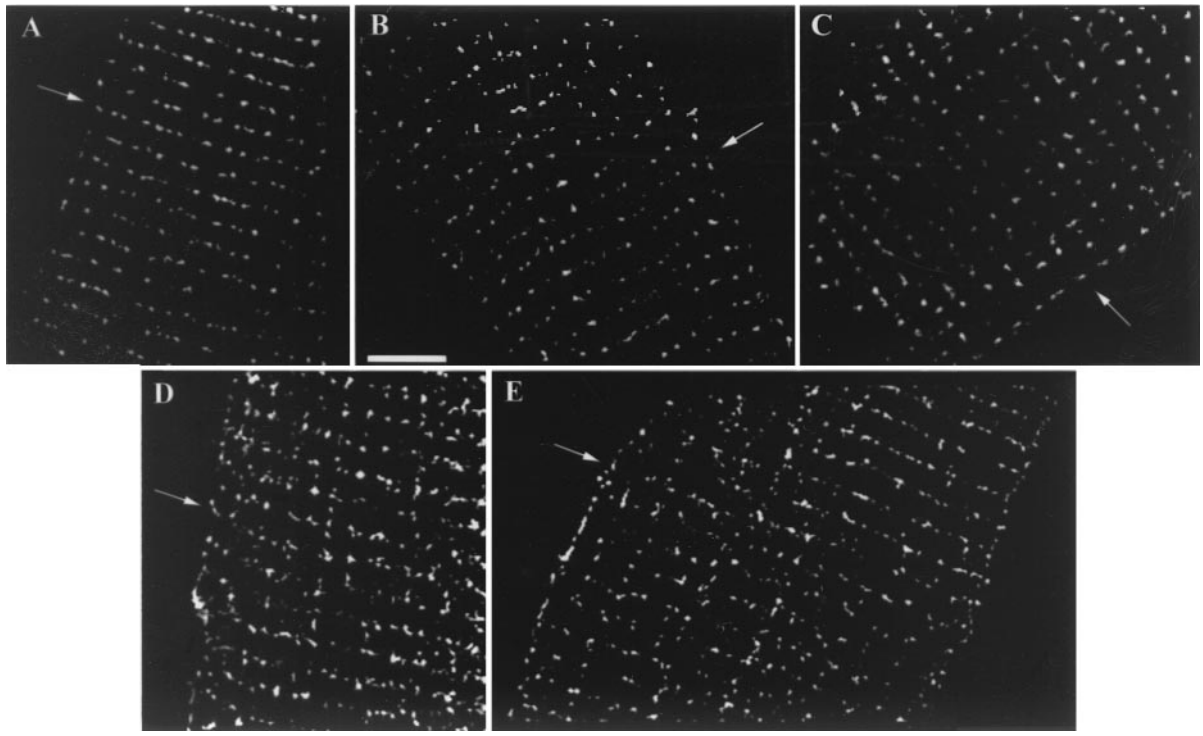

FIGURE 3 Images of four planes (1 μm in depth) from myocytes showing the distribution of each of the labeled proteins. After acquisition, the images were deconvolved and thresholded. Scale bar is 5 μm; arrows point to the surface of the cell and to a *z* line. (*A*) Ryanodine receptor; note the lack of distinct edges to the cell. (*B*) α_{1C} subunit of the L type Ca^{2+} channel. (C) Calsequestrin. (*D*) Na^+/Ca^{2+} exchanger. (*E*) Na^+ channel.

and voltage-gated Na^+ channels in t-tubule membranes suggests that the tubules have three distinct structural domains: one containing L-type Ca^{2+} channels positioned opposite ryanodine receptors in the closely apposed SR membrane, whose principal function is Ca^{2+}-induced Ca^{2+} release; a second containing Na^+/Ca^{2+} exchangers for Ca^{2+} extrusion; and a third containing voltage-gated Na^+ channels for rapid depolarization.

Imaging

The effectiveness of our analytical techniques was demonstrated by three internal controls: first, the level of co-incidence when we labeled the ryanodine receptor twice was identical with both secondary antibodies and defined the empirical maximum that could be recorded (63%). Second, the L-type Ca^{2+} channels and ryanodine receptors, which previous experiments have indicated are co-localized (Carl et al., 1995; Sun et al., 1995), had a level of co-incidence close to that maximum. Last, the measured co-incidence of calsequestrin and ryanodine receptors, which are known to be functionally and physically coupled (Guo and Campbell, 1995), is also near the maximum. Taken together, these results indicate the cross-correlation and strict co-localization requirements were both reasonable and effective.

Subcellular distribution of proteins

The level of co-incidence between the L-type Ca^{2+} channels and ryanodine receptors was significantly higher than that between the ryanodine receptors and L-type Ca^{2+} channels. We attribute this difference to there being more voxels displaying label specific for the ryanodine receptor than for the L-type Ca^{2+} channel (Table 1) and hypothesize that those ryanodine receptors without associated L-type Ca^{2+} channels are located in corbular SR; corbular SR has been identified in mammalian ventricle, although its functional significance is uncertain (Jorgensen et al., 1985). The distribution of all of the ryanodine receptors, both junctional and corbular, was almost exclusively in the vicinity of the *z* line, as has been suggested by scanning electron microscopy (Ogata and Yamasaki, 1990). We have suggested that ryanodine receptors without associated L-type Ca^{2+} channels are present in corbular SR. This conclusion was strengthened by the fact that, at the limit of our ability to measure, calsequestrin was always accompanied by ryanodine receptors, and vice versa. This implies that ryanodine receptors that are not coupled to L-type Ca^{2+} channels are coupled to internal Ca^{2+} stores, which could be consistent with their hypothesized role as secondary sites of Ca^{2+} release (Niggli and Lederer, 1990).

The images in Figs. 2 and 3 show little labeling of L-type Ca^{2+} channels, ryanodine receptors, or calsequestrin on the cell surface other than at the end of the *z* lines at or near the mouth of the t-tubules. A two dimensional image of any of these proteins produces a highly regular array of spots along the length and width of the cell, separated by distances corresponding to the length of a sarcomere and the width of a myofibril respectively, but as the images in Fig. 2, *A–C* demonstrate, there is no regular pattern of distribution along the *z* axis.

In contrast to this is the labeling seen with both the Na^+/Ca^{2+} exchanger and voltage-gated Na^+ channels. Spots of fluorescence specific for either of these proteins were seen largely along, but not limited to, the *z* line. As the images displayed in Figs. 2 *E*, 3 *D*, and 3 *E* show, there are, in places, lines of fluorescent spots running parallel to the long axis of the cells. We see similarities in this staining pattern with the complex anatomy of the t-tubular system in rat ventricular myocytes. This system, which is formed by invaginations of the sarcolemma, has axial elements that run parallel to the long axis of the cell for several sarcomeres (Forssmann and Giradier, 1970; Sommer and Waugh, 1976; Ogata and Yamasaki, 1990). Assuming that the distribution of both the Na^+/Ca^{2+} exchanger and voltage-gated Na^+ channels is limited to surfaces that connect with the extracellular space, the most likely explanation for our observation is that both proteins are located on these axial elements.

The Na^+/Ca^{2+} exchanger and the voltage-gated Na^+ channels have both been previously localized in t-tubules at the *z* lines of guinea pig, rat, and rabbit ventricular myocytes (Frank et al., 1992; Kieval et al., 1992; Chen et al., 1995; Cohen, 1996). Our results agree with this, but in addition we see these proteins distributed along axial elements of the tubules. As Fig. 3 *E* demonstrates, the voltage-gated Na^+ channels are also located on the sarcolemma between the *z* lines, the only one of the proteins examined to have a significant presence in this location. There is disagreement as to whether the Na^+/Ca^{2+} exchanger is also located here (Frank et al., 1992; Kieval et al., 1992), but our images suggest that the majority is at the mouth of t-tubules. Analytical electron microscopy has concluded that roughly half of the membrane area in the t-system is involved in forming junctions with the SR (Page, 1978). Since the exchanger and the Na^+ channel are minimally co-localized, our results indicate that the other half is divided into at least two structural domains. One contains the Na^+/Ca^{2+} exchanger, whose primary function is most likely extrusion of Ca^{2+} from the myocyte (Bridge et al., 1990; Crespo et al., 1990), the other the voltage-gated Na^+ channel, whose function, at least in part, is rapid membrane depolarization and spread of the action potential.

All of the proteins examined were localized to discrete regions of the sarcolemma/t-tubule system or SR; none were uniformly distributed in the compartment in which they were located. Previous studies in neurons have indicated that ion channels are localized in plasma membranes through binding to cytoskeletal elements, and that this localization is critical for cell function (Sheng et al., 1992; Wang et al., 1993). In cardiomyocytes it has been reported that Na^+/Ca^{2+} exchangers bind to the cytoskeletal protein ankyrin (Li et al., 1993) and that Na^+ channels bind to dystrophin through syntrophin at the sarcolemma (Gee et al., 1998). Therefore, the patterns of distribution that we have observed may reflect underlying cytoskeletal interactions that are essential in localizing the proteins.

Implications for EC coupling

Our results clearly indicate that Na^+/Ca^{2+} exchangers and Na^+ channels are located outside of the dyads containing the ryanodine receptors and Ca^{2+} channels. The impact of these results on theories of EC coupling is dependent on the assumed structure of the fuzzy space. We have considered two possible architectures supported by experimental evidence.

One possibility is that the fuzzy space is limited to the junctional regions between the apposed membrane surfaces of the t-tubule and the SR. This model is supported by electrophysiological observations suggesting that the L-type Ca^{2+} channels and ryanodine receptors are in a different domain from the Na^+/Ca^{2+} exchangers (Adachi-Akahane et al., 1996). In addition, this anatomically restricted space provides the architecture for CICR via L-type Ca^{2+} channels and is an obvious candidate. Our results show that only 3.1% of the Na^+ channels and 3.6% of the Na^+/Ca^{2+} exchangers co-localize with ryanodine receptors, indicating that neither is located to a significant extent within junctional regions. If all of the junctions containing Na^+ channels contained Na^+/Ca^{2+} exchangers, it would still represent an insignificant fraction of the total and could not produce phasic contractions. In this model of the fuzzy space the vast majority of Na^+ channels and Na^+/Ca^{2+} exchangers would face, and communicate with, the bulk myoplasm. Reversal of the exchanger via an increase in myoplasmic Na^+ concentration would then be impossible, given the sizes of the Na^+ current and the cell (Lederer et al., 1990). It is equally unlikely that Na^+ influx could produce a local Na^+ concentration high enough to reverse the exchanger, as there is virtually no coincidence of these molecules. Ca^{2+} entering through the slip mode conductance would also enter the bulk myoplasm. Experimental data indicate that this mode results in undetectable changes in the myoplasmic calcium concentration (Santana et al., 1998) and should therefore be unable to activate ryanodine receptors. We conclude that if the fuzzy space is restricted to the region of t-tubule SR junctions, triggering CICR by either reverse-mode entry of Ca^{2+} or slip mode conductance seems improbable.

A second possibility is that the fuzzy space encompasses the dyads, Na^+ channels, and Na^+/Ca^{2+} exchangers. This model is supported by a series of observations: differences

between the bulk myoplasmic [Ca^{2+}] and the [Ca^{2+}] sensed by the exchanger (Trafford et al., 1995); a discrete subsarcolemmal compartment of Ca^{2+} that equilibrates only with the exchanger (Langer and Rich, 1992); and subsarcolemmal microdomains of elevated [Ca^{2+}] (Gallitelli et al., 1999). It is unclear whether this fuzzy space is continuous or not. Wendt-Gallitelli et al. (1993) observed that different regions of a 20-nm-thick subsarcolemmal space displayed distinct Na^+ concentrations, indicating that there were multiple, separate, sites where diffusion of Na^+ was restricted. In either of these models the Ca^{2+} ions must diffuse at least 122 nm (our results) to junctional or corbular SR so as to trigger Ca^{2+} release. Since both the amount of Ca^{2+} entering the cell (via slip-mode or reverse-mode) and the volume of the fuzzy space are unknown, it is impossible to give a definitive answer as to whether the Ca^{2+} concentration reached at the ryanodine receptors would be sufficient to trigger contraction.

We conclude that neither reverse mode operation of the exchanger nor slip mode conductance can trigger CICR if the junctional regions are the only space of restricted diffusion. A continuous or disjoint subplasmalemmal space of restricted diffusion might enable either mechanism to trigger CICR.

There is evidence that the density and characteristics of the exchanger differs between species (Sham et al., 1995), therefore the molecular architecture that we have observed in the rat may not apply to other animals. In addition, there is evidence for a TTX sensitive Ca^{2+} current different from the slip mode conductance (Aggarwal et al., 1997; Nargeot, 2000), though it is not clear what contribution this might make. This pathway, the species differences, and the structure of the fuzzy space require further investigation.

The authors thank the following individuals for their generous gifts of antibody: Dr. K. Philipson for anti-Na^+/Ca^{2+} exchange, Dr. G. Meissner for anti-RyR, Dr. K. Campbell for anti-calsequestrin, Dr. W. Catterall for anti-α_{1C}, and Dr. S. Cohen for anti-rH1. We also thank the Biomedical Imaging Group at the University of Massachusetts for analysis, visualization, and deconvolution software, and for many helpful discussions. In particular, E.D.W.M. would like to dedicate this work to his late friend and mentor, Dr. Fredric Fay.

This work was supported by a Research Traineeship from the Heart and Stroke Foundation of British Columbia and the Yukon (to P.D.) and by grants from the Medical Research Council of Canada and HSFBC&Y (to E.D.W.M.).

REFERENCES

Adachi-Akahane, S., L. Cleemann, and M. Morad. 1996. Cross-signaling between L-type Ca^{2+} channels and ryanodine receptors in rat ventricular myocytes. *J. Gen. Physiol.* 108:435–454.

Aggarwal, R., S. R. Shorofsky, L. Goldman, and C. W. Balke. 1997. Tetrodotoxin-blockable calcium currents in rat ventricular myocytes; a third type of cardiac cell sodium current. *J. Physiol.* 505:353–369.

Bouchard, R. A., R. B. Clark, and W. R. Giles. 1993. Role of sodium-calcium exchange in activation of contraction in rat ventricle. *J. Physiol.* 472:391–413.

Bridge, J. H., J. R. Smolley, and K. W. Spitzer. 1990. The relationship between charge movements associated with I_{Ca} and $I_{Na\text{-}Ca}$ in cardiac myocytes. *Science.* 248:376–378.

Carl, S. L., K. Felix, A. H. Caswell, N. R. Brandt, W. J. Ball, Jr., P. L. Vaghy, G. Meissner, and D. G. Ferguson. 1995. Immunolocalization of sarcolemmal dihydropyridone receptor and sarcoplasmic reticular triadin and ryanodine receptor in rabbit ventricle and atrium. *J. Cell Biol.* 129:673–682.

Carrington, W. E., K. E. Fogarty, and F. S. Fay. 1990. 3D fluorescence imaging of single cells using image restoration. *In* Noninvasive Techniques in Cell Biology. J. K. Foskett and S. Grinstein, editors. Wiley-Liss, New York. 53–72.

Chen, F., G. Mottino, T. S. Klitzner, K. D. Philipson, and J. S. Frank. 1995. Distribution of the Na^+/Ca^{2+} exchange protein in developing rabbit myocytes. *Am. J. Physiol. Cell Physiol.* 268:C1126–C1132.

Cohen, S. A. 1996. Immunocytochemical localization of rH1 sodium channel in adult rat heart atria and ventricle. Presence in terminal intercalated disks. *Circulation.* 94:3083–3086.

Cohen, S. A., and L. K. Levitt. 1993. Partial characterization of the rH1 sodium channel protein from rat heart using subtype-specific antibodies. *Circ. Res.* 73:735–742.

Crespo, L. M., C. J. Grantham, and M. B. Cannell. 1990. Kinetics, stoichiometry and role of Na-Ca exchange mechanism in isolated cardiac myocytes. *Nature.* 345:618–621.

Fabiato, A. 1985. Time and calcium dependence of activation and inactivation of calcium-induced release of calcium from the sarcoplasmic reticulum of a skinned canine cardiac Purkinje cell. *J. Gen. Physiol.* 85:247–289.

Forssmann, W. G., and L. Giradier. 1970. A study of the T system in rat heart. *J. Cell Biol.* 44:1–19.

Frank, J. S., G. Mottino, D. Reid, R. S. Molday, and K. D. Philipson. 1992. Distribution of the Na^+-Ca^{2+} exchange protein in mammalian cardiac myocytes: an immunofluorescence and immunocolloidal gold-labeling study. *J. Cell Biol.* 117:337–345.

Gallitelli, M. F., M. Schultz, G. Isenberg, and F. Rudolf. 1999. Twitch-potentiation increases calcium in peripheral more than in central mitochondria of guinea-pig ventricular myocytes. *J. Physiol.* 518:433–447.

Gee, S., R. Madhaven, S. Levinson, J. H. Caldwell, R. Sealock, and S. C. Froehner. 1998. Interaction of muscle and brain sodium channels with multiple members of the syntrophin family of dystrophin-associated proteins. *J. Neurosci.* 18:128–137.

Guo, W., and K. P. Campbell. 1995. Association of triadin with the ryanodine receptor and calsequestrin in the lumen of the sarcoplasmic reticulum. *J. Biol. Chem.* 270:9027–9030.

Hell, J. W., C. T. Yokoyama, S. T. Wong, C. Warner, T. P. Snutch, and W. A. Catterall. 1993. Differential phosphorylation of two size forms of the neuronal class C L-type calcium channel α_1 subunit. *J. Biol. Chem.* 268:19451–19457.

Jorgensen, A. O., and K. P. Campbell. 1984. Evidence for the presence of calsequestrin in two structurally different regions of myocardial sarcoplasmic reticulum. *J. Cell Biol.* 98:1597–1602.

Jorgensen, A. O., A. C. Shen, and K. P. Campbell. 1985. Ultrastructural localization of calsequestrin in adult rat atrial and ventricular muscle cells. *J. Cell Biol.* 101:257–268.

Kieval, R. S., R. J. Bloch, G. E. Lindenmayer, A. Ambesi, and W. J. Lederer. 1992. Immunofluorescence localization of the Na-Ca exchanger in heart cells. *Am. J. Physiol. Cell Physiol.* 263:C545–C550.

Lai, F. A., Q. Y. Liu, L. Xu, A. el-Hashem, N. R. Kramarcy, R. Sealock, and G. Meissner. 1992. Amphibian ryanodine receptor isoforms are related to those of mammalian skeletal or cardiac muscle. *Am. J. Physiol. Cell Physiol.* 263:C365–C372.

Langer, G. A., and T. L. Rich. 1992. A discrete Na-Ca exchange-dependent Ca compartment in rat ventricular cells: exchange and localization. *Am. J. Physiol. Cell Physiol.* 262:C1149–C1153.

Leblanc, N., and J. R. Hume. 1990. Sodium current-induced release of calcium from cardiac sarcoplasmic reticulum. *Science.* 248:372–376.

Lederer, W. J., E. Niggli, and R. W. Hadley. 1990. Sodium-calcium exchange in excitable cells: fuzzy space. *Science.* 248:283.

Levi, A. J., P. Brooksby, and J. C. Hancox. 1993. A role for depolarization induced calcium entry on the Na-Ca exchange in triggering intracellular calcium release and contraction in rat ventricular myocytes. *Cardiovasc. Res.* 27:1677–1690.

Li, Z., E. P. Burke, J. S. Frank, V. Bennett, and K. D. Philipson. 1993. The cardiac Na^+-Ca^{2+} exchanger binds to the cytoskeletal protein ankyrin. *J. Biol. Chem.* 268:11489–11491.

Moore, E. D. W., E. F. Etter, K. D. Philipson, W. A. Carrington, K. E. Fogarty, L. M. Lifshitz, and F. S. Fay. 1993. Coupling of the Na^+/Ca^{2+} exchanger, Na^+/K^+ pump and sarcoplasmic reticulum in smooth muscle. *Nature.* 365:657–660.

Nargeot, J. 2000. A tale of two (calcium) channels. *Circ. Res.* 86:613–615.

Niggli, E., and W. J. Lederer. 1990. Voltage-independent calcium release in heart muscle. *Science.* 250:565–568.

Ogata, T., and Y. Yamasaki. 1990. High-resolution scanning electron microscopic studies on the three-dimensional structure of the transverse-axial tubular system, sarcoplasmic reticulum and intercalated disc of the rat myocardium. *Anat. Rec.* 228:277–287.

Page, E. 1978. Quantitative ultrastructural analysis in cardiac membrane physiology. *Am. J. Physiol. Cell Physiol.* 235:C147–C158.

Rodrigues, B., and D. L. Severson. 1997. Preparation of cardiomyocytes. *In* Biochemical Techniques in the Heart. J. H. McNeil, editor. CRC Press, Boca Raton, FL. 101–115.

Santana, L. F., A. M. Gomez, and W. J. Lederer. 1998. Ca^{2+} flux through promiscuous cardiac Na^+ channels: slip-mode conductance. *Science.* 279:1027–1033.

Satoh, H., K. S. Ginsburg, K. Qing, H. Terada, H. Hayashi, and D. M. Bers. 2000. KB-R7943 block of Ca^{2+} influx via Na^+/Ca^{2+} exchange does not alter twitches or glycoside inotropy but prevents Ca^{2+} overload in rat ventricular myocytes. *Circulation.* 101:1441–1446.

Sham, J. S. K., L. Cleemann, and M. Morad. 1992. Gating of the cardiac Ca^{2+} release channel: the role of Na^+ current and Na^+-Ca^{2+} exchange. *Science.* 255:850–853.

Sham, J. S. K., S. N. Hatem, and M. Morad. 1995. Species differences in the activity of the Na^+-Ca^{2+} exchanger in mammalian cardiac myocytes. *J. Physiol.* 488:623–631.

Sheng, M., M.-L. Tsaur, Y. N. Jan, and L. Y. Jan. 1992. Subcellular segregation of two A-type K^+ channel proteins in rat central neurons. *Neuron.* 9:271–284.

Sommer, J. R., and R. A. Waugh. 1976. The ultrastructure of the mammalian cardiac muscle cell—with special emphasis on the tubular membrane systems. *Am. J. Pathol.* 82:192–231.

Sun, X. H., F. Protasi, M. Takahashi, H. Takeshima, D. G. Ferguson, and C. Franzini-Armstrong. 1995. Molecular architecture of membranes involved in excitation-contraction coupling of cardiac muscle. *J. Cell Biol.* 129:659–671.

Toffolo, R. L., and C. D. Ianuzzo. 1994. Myofibrillar adaptations during cardiac hypertrophy. *Mol. Cell. Biochem.* 131:141–149.

Trafford, A. W., M. E. Diaz, S. C. O'Neill, and D. A. Eisner. 1995. Comparison of subsarcolemmal and bulk calcium concentration during spontaneous calcium release in rat ventricular myocytes. *J. Physiol.* 488:577–586.

Wang, H., D. D. Kunkel, T. M. Martin, P. A. Schwartzkroin, and B. L. Tempel. 1993. Heteromultimeric K+ channels in terminal and juxtaparanodal regions of neurons. *Nature.* 365:75–79.

Wasserstrom, J. A., and A. M. Vites. 1996. The role of Na^+-Ca^{2+} exchange in activation of excitation-contraction coupling in rat ventricular myocytes. *J. Physiol.* 493:529–542.

Wendt-Gallitelli, M. F., T. Voight, and G. Isenberg. 1993. Microheterogeneity of subsarcolemmal sodium gradient. Electron probe microanalysis in guinea pig ventricular myocytes. *J. Physiol.* 472:33–44.